

Improved structural and mechanical performance of iron oxide scaffolds freeze cast under oscillating magnetic fields

Josh R. Fernquist, Henry C. Fu, Steven E. Naleway*

University of Utah, Department of Mechanical Engineering, United States

ARTICLE INFO

Keywords:

Freeze casting
Helmholtz coil
Uniform magnetic field
Oscillating magnetic field
Wobbling magnetic field

ABSTRACT

Manufacturing processes yielding stronger, yet lighter structures are sought for in many industries and scientific applications. Freeze casting is a fabrication process that offers a way to achieve these strong, lightweight structures, but only in a single direction (the direction of the templating-ice growth). Applying a uniform magnetic field to these structures allows for increased strength in an additional direction, thus allowing for them to be applied in a variety of complex loading environments. Using a Helmholtz coil, it is possible to apply weak, uniform fields in any direction, magnitude, or frequency. Previous research using Helmholtz coils has shown that an applied field can increase strength through microstructural alignment, but the limited field strength reduces the applicability of these materials. To mitigate this, an oscillating field (i.e., a stronger magnetic field in a single direction with a weaker alternating field in an orthogonal direction) of various magnitudes of oscillation during the fabrication of freeze-cast materials was applied using Helmholtz coils. These oscillating magnetic fields led to an increase of strength of up to 2.5x compared to materials fabricated with either no applied field or a non-oscillating applied field due to increased alignment and thickness of the lamellar walls. This demonstrates that increased material response can be induced through the application of an oscillating field without increasing the maximum magnetic field strength.

1. Introduction

Freeze casting is a fabrication process for porous materials that has been extensively researched over the past 20 years [1,2]. This is due in large part to its ease of use and ability to fabricate porous materials from a wide range of constituents, from metals [3–6] and polymers [7–11] to ceramics [12–15] and composites [16,17]. The freeze casting process consists of:

1. Creating and mixing a slurry with one or multiple solid loadings, along with binders, dispersants, and a liquid freezing agent.
2. Directionally freezing said slurry, for example, by pouring into a mold connected to a cold finger. The cold finger is then submerged in a cold bath, which causes the liquid freezing agent to directionally solidify and template the material.
3. Sublimating the grown ice crystals, resulting in a green body.
4. Finally, densifying the green bodies (e.g., by sintering in a furnace), thus allowing the green bodies to form into porous scaffolds where the porosity has been templated by the grown ice crystals.

In addition to the variety of constituents that have been used in freeze casting, many different factors having been studied in the freeze-casting fabrication process to control the structure and properties of the resultant materials. These factors include the use of slurry additives [18–22], varying freezing rates [23–25], varying freezing directions [26–32], and the application of external forces (magnetic, electric, acoustic) [15,32–37]. The first two factors can be classified as intrinsic factors (i.e., a factor that is changed internally), while the latter two are considered extrinsic factors (i.e., a factor that is applied externally) [38]. Of particular interest, recent research has shown that applied magnetic fields have been able to effect significant increases in the mechanical properties through microstructural alignment [15,21,34–36].

The basic freeze-casting process, without the use of extrinsic factors such as applied magnetic fields, creates structures that are strong in the ice-growth direction, while weak in the other two orthogonal directions [21,34]. Application of magnetic fields during the fabrication process has been shown to lead to increased strength in the other orthogonal directions, with increases in strength up to 300% [36,39]. To enact these results, the magnetic field is applied during the freezing of the slurry

* Corresponding author.

E-mail address: steven.naleway@mech.utah.edu (S.E. Naleway).

<https://doi.org/10.1016/j.ceramint.2022.02.032>

Received 4 November 2021; Received in revised form 18 January 2022; Accepted 4 February 2022

Available online 9 February 2022

0272-8842/© 2022 Elsevier Ltd and Techna Group S.r.l. All rights reserved.

(step 2 above), as this is when the particles, which are suspended in the liquid freezing agent, are most susceptible to alignment [36,39,40]. A majority of these studies utilized permanent magnet setups [21,33–35]. These setups allow for fields of large field strength magnitudes to be produced, but at the cost of creating a high magnetic field gradient [37]. This gradient is generated because the field strength near the magnets is much greater than the field strength at the center of the setup [37]. Therefore, these permanent magnet-based setups present a critical issue: particles that are susceptible to magnetic fields will be pulled to the surface of the green bodies closest to the permanent magnets, thus causing plating [35]. This plating leads to strong surface material, while weakening the interior of the structures, thus limiting the bulk strength of the resultant material.

To combat this, recent research demonstrated the ability to impact freeze-casting with magnetic field setups that generated uniform fields with little to no magnetic field gradient [36]. This allowed for materials to be created without causing particle migration to the surface (i.e., plating), with only alignment of the particles in the slurries to create structures that are stronger in orthogonal directions in addition to the ice-growth direction. To create these setups, Helmholtz coils have been used [36]. Helmholtz coils are pairs of electromagnets that are able to apply a nearly-constant magnetic field [36,41]. In addition, multiple Helmholtz coils can be orthogonally arranged to allow for fields of differing directions and magnitudes to be applied simultaneously. The most common version of this is a tri-axial Helmholtz coils, where three coils are nested together, each pointing in a different orthogonal direction, thus allowing for a field to be generated in any direction. Of note, previous research in controlling freeze-cast materials with a tri-axial Helmholtz coils has applied two or more fields orthogonal to one another to create complex fields such as a diagonal field [39] and rotating fields [40], both of which allowed for complex control over the freeze-casting process. In these cases, materials have been fabricated using ferromagnetic constituents, e.g. iron oxide, as these materials are highly susceptible to the low magnitude magnetic fields that are generated [41].

While Helmholtz coils are capable of applying uniform magnetic fields in any desired direction, they are unable to apply magnetic fields of similar magnitudes as permanent magnets, with Helmholtz coils-generated magnetic fields limited in current reports to ~ 10 mT [34, 36]. To expand the benefits of Helmholtz coils in freeze casting, there is a need to increase the material response despite the low magnetic field strengths. Applying multiple magnetic fields simultaneously has been shown to further increase the material response and lead to enhanced

organization in the structures [39,40]. To this end, this research will also focus on applying multiple fields simultaneously during the freeze-casting process. One magnetic field will be applied in one direction, at a high magnitude, hereby referred to as a “constant field”, while a second magnetic field will be applied simultaneously, orthogonal to the first field, at a much lower magnitude, and alternating in field direction at a certain frequency, hereby referred to as an “alternating field”. The combination of these magnetic fields, hereby referred to as an “oscillating magnetic field” were demonstrated to provide enhanced material response when combined with freeze casting.

2. Materials and methods

2.1. Generation of constant magnetic field

Differing from previous studies [34,35], the fields applied in this study have negligible magnetic field gradient, i.e. at a given point in time the field is effectively the same across all points of the field. A tri-axial Helmholtz coils was used to produce this result (Fig. 1a). This coil was utilized and manufactured in a previous study [39]. It was tested and shown to provide accurate fields and field types with very low magnetic field gradient, as denoted by a negligible range of error [39]. The coils are controlled via computer using the LabVIEW software, allowing the user to specify magnitude, direction, and frequency of field in any of the three orthogonal directions, those being the x-direction, y-direction, and z-direction (as defined in Fig. 1a). The y-direction corresponds to the ice-growth direction in this research.

2.2. Sample preparation

Each scaffold was prepared by first mixing a slurry together. The slurries consisted of the solid loading compound Fe_3O_4 (Iron Oxide II/III) from ACROS Organics (Pittsburgh, PA, USA) at 10 wt%, binders polyvinyl alcohol (PVA) at 1 wt% and polyethylene glycol (PEG) at 1 wt%, additive Octanol at 0.435 wt% as an anti-foaming agent, and the dispersant Darvan 811 at 1 wt%. Fe_3O_4 was used due to previous success with freeze casting under magnetic fields with this material and due to its high magnetic susceptibility [36,39,40]. Each slurry was 8 mL in total volume. The slurries were then mixed in a Sper Scientific sonicator (Scottsdale, Arizona, USA) for 12 min. The mixed slurry was then immediately poured into a PVC mold atop a cold finger sitting in a bath of liquid N_2 (as shown in Fig. 1b). A thermocouple and band heater were attached to the cold finger to monitor the temperature and to decrease it

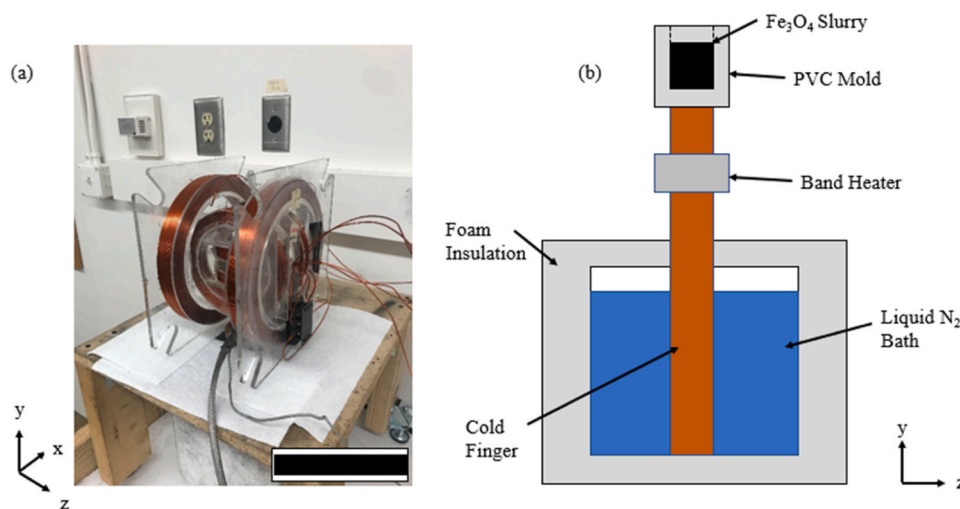


Fig. 1. (a) Trimetric view of Helmholtz coil along with the coordinate system used herein. The large coils correspond with the z-direction, the medium coils with the x-direction, and the small coils with the y-direction or ice-growth direction. (b) Detailed view of the freeze-casting setup. The Helmholtz coils are placed over the PVC mold and slurry during the freezing process. The scale bar corresponds to 10 cm.

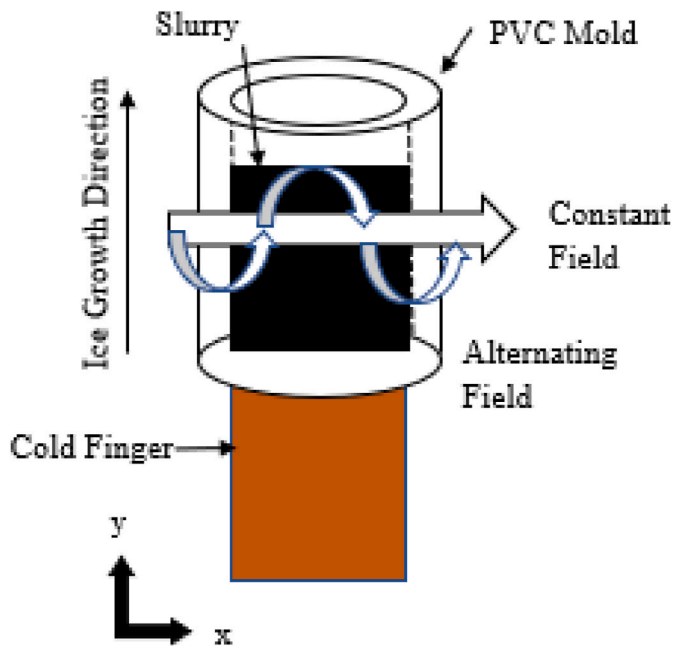


Fig. 2. Visual representation of the alternating field applied in conjunction with a constant field during the freeze-casting process.

at a constant rate of $10\text{ }^{\circ}\text{C per min}^{-1}$. All slurries were directionally frozen in the y-direction. A total of 50 scaffolds were fabricated, with 10 being fabricated under each of five different magnetic field types (with the fields visualized in Fig. 2):

- No Field: no field was applied during the freeze-casting process.
- Constant Field: field was applied in the x-direction at a constant magnitude of 7.8 mT.
- 10% Oscillation: a field was applied in the x-direction at a constant magnitude of 7.8 mT, along with an alternating field in the y-direction ranging between 0.78 mT and -0.78 mT at 5 rpm.
- 20% Oscillation: a field was applied in the x-direction at a constant magnitude of 7.8 mT, along with an alternating field in the y-direction ranging between 1.56 mT and -1.56 mT at 5 rpm.
- 30% Oscillation: a field was applied in the x-direction at a constant magnitude of 7.8 mT, along with an alternating field in the y-direction ranging between 2.34 mT and -2.34 mT at 5 rpm.

All fields were oscillated at 5 rpm. This frequency was chosen based on preliminary experiments where various frequencies were tested and 5 rpm showed the most promising results for aligning particles. In all cases, the fields were applied throughout the entire freezing process. After freezing the slurries, they were all lyophilized at 0.047 mBar and $51\text{ }^{\circ}\text{C}$ in a Labconco Free Zone 1 freeze drier (Kansas City, MO, USA) to sublimate all the ice crystals from the scaffolds. Once lyophilized, the green bodies were placed in an open-air Keith KSK-12 1700 furnace

2.3. Mechanical testing

Each scaffold was mechanically tested on an Instron 5967 load frame with an Instron 30 kN load cell (Norwood, MA, USA). The scaffolds were prepared for mechanical testing by cutting 4 cubes from the midsection of each scaffold (see Fig. 3). From each scaffold, two of the cubes were compressed normal to the y-direction or ice-growth direction, and two cubes were compressed normal to the x-direction, or the direction of the applied constant magnetic field. Each cube was approximately 4 mm in height with an approximate cross-sectional area of 19 mm^2 . Each cube was compressed at a crosshead speed of 1 mm min^{-1} . The ultimate compression strength (UCS) and modulus of elasticity (E) were recorded during each test with the UCS being recorded at the highest engineering compression stress and the E being recorded at the elastic limit as the slope of the linear-elastic region of the stress-strain curve. The results of this were 19 compression tests completed in both the x-direction and y-direction for each field type.

2.4. Material characterization

To view and characterize the microstructures of the scaffolds, images were taken of scaffolds for each field type using a scanning electron microscope (SEM) (FEI Quanta 600 FG, Hillsboro, Oregon, USA). For each scaffold, a cross-section $\sim 2\text{ mm}$ thick was sectioned and all images were taken on the x-z face, normal to the ice-growth direction (see Fig. 3). 20 total scaffolds were imaged with 4 at each magnetic field type. These images were analyzed using the Image J software. This software allowed for the measurement of wall thickness, area porosity, pore area, pore major axis length, and pore minor axis length. All measurements were made on 250x magnification images. The results of these were 320 measurements of each field type for the wall thickness, while 5000 measurements were taken for the area porosity, average pore size, and length of the major and minor axis. The wall thickness, major axis, and minor axis were all recorded in units of micrometers (μm), while the average pore size was recorded in units of micrometers squared (μm^2), and lastly the area porosity was recorded in a unitless percentage (%).

The lamellar wall alignment was analyzed using ImageJ software to further quantify how the microstructure changed as a function of the field type. The images were analyzed along the x-z face. This was done by dividing the face into eight separate sectors of angles, as used in previous studies [21,39]. Each of the eight sectors is as follows: $-67.5^{\circ} \pm 11.25^{\circ}$, $-45^{\circ} \pm 11.25^{\circ}$, $-22.25^{\circ} \pm 11.25^{\circ}$, $0^{\circ} \pm 11.25^{\circ}$, $22.25^{\circ} \pm 11.25^{\circ}$, $45^{\circ} \pm 11.25^{\circ}$, $67.5^{\circ} \pm 11.25^{\circ}$, and $90^{\circ} \pm 11.25^{\circ}$, with the 0° corresponding with the x-direction (direction of the applied constant magnetic field) and the 90° corresponding with the z-direction (perpendicular to the applied constant magnetic field) as shown in Fig. 4a. Each image had its total area measured, then was subdivided into smaller sections whose lamellar walls were pointing in one of the eight sector directions. For each scaffold the percent area of each subsection whose lamellar walls were pointing in each sector direction was calculated as the following:

$$\% \text{ area in sector range } n = \frac{\text{total imaged scaffold surface area aligned with } n}{\text{total imaged surface area of scaffold}} \times 100$$

(Pico Rivera, CA, USA) and sintered at $1150\text{ }^{\circ}\text{C}$ for 20 min, with heating and cooling rates of $2\text{ }^{\circ}\text{C min}^{-1}$, resulting in solid scaffolds that could then be mechanical tested and analyzed.

An example of calculating this areas can be seen in Fig. 4b. The results of this were eight images analyzed for each field type, for a total of 40 images analyzed using this method.

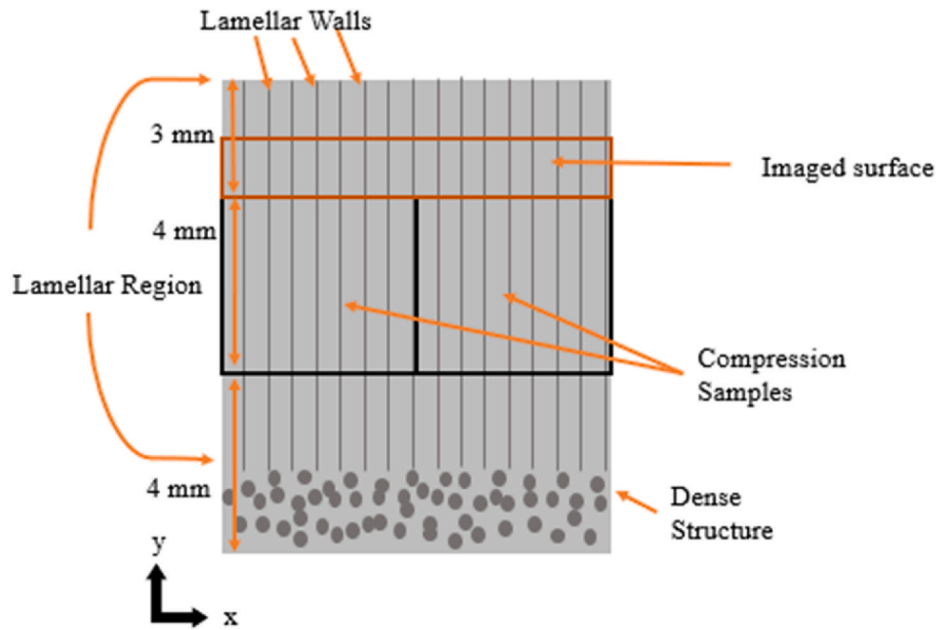


Fig. 3. An illustrated, cross-sectional diagram of a scaffolds and what samples were used. The bottom ~4 mm of the scaffold are removed due to the formation of dense structures. The compression samples begin ~4 mm from the bottom of the scaffold and are ~4 mm in height. Above the compression sample, ~2 mm of lamellar material is removed and used for imaging. All scaffolds were analyzed in the lamellar region above the dense structure.

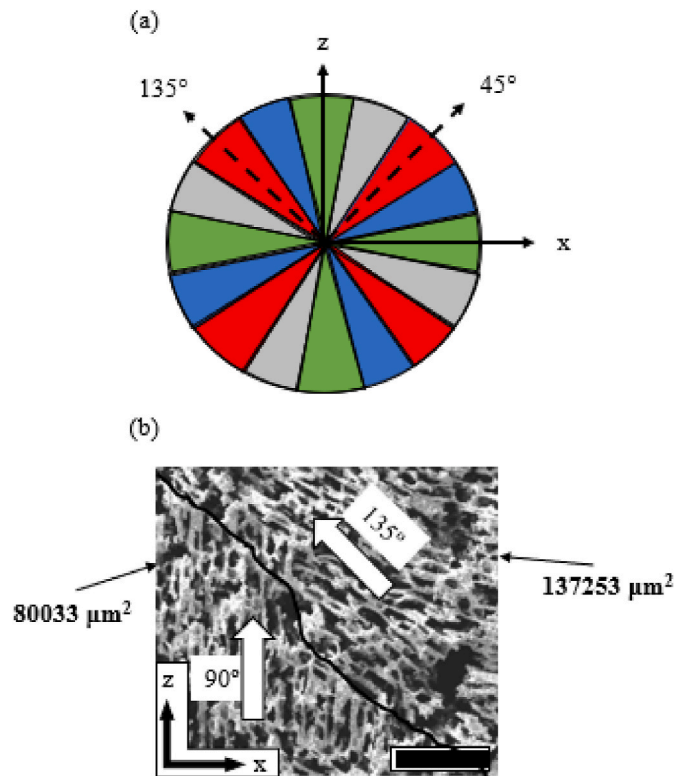


Fig. 4. (a) Visual representation of the eight defined sectors in the x-z plane where 0° corresponds with the x-direction and 90° corresponds with the z-direction. (b) An example SEM image with areas divided into the sectors that the lamellar wall directions correspond to. Figure was inspired by Nelson et al. [39].

2.5. Statistical analysis

A statistical analysis was run over the mechanical and image data of the scaffolds using a One-way ANOVA test in R-studio software. The five different field types were considered, those being No Field, Constant Field, 10% Oscillation, 20% Oscillation, or 30% Oscillation. Each test was run using a significant difference of $\alpha = 0.05$. If the test returned with a p-value less than the α value, then it was assumed that there were statistically significant differences in the data in question. If statistical significance was identified, a Tukey’s Honest Significant Difference (HSD) test was then run on the data to view the significance of individual pair-wise comparisons. The same value of $\alpha = 0.05$ was used for these test.

3. Results and discussion

3.1. Expected effects of oscillating fields

In metallurgy, the practice of annealing is quite common [42–45]. This practice of heat treating entails taking a metal and heating it above its crystallization temperature, maintaining that temperature for a specific amount of time, then slowly cooling it [46]. As the metal cools down, it forms its crystalline structure, and due to the slow cooling rate, it is able to form more bonds and bridges, and decrease dislocations, thus changing the hardness and strength of the metal [47]. The metal is given the energy (through increasing the temperature beyond the crystallization temperature) to reform and settle in a low energy state, that being a crystalline structure [47]. Without this added energy through an increase of temperature, the metal is unable to achieve this low energy state, and remains in a higher, less organized energy state [47]. The application of oscillating magnetic fields during freeze casting can be viewed as an analog of annealing. When the magnetic field is applied, the ferromagnetic particles will tend to align with the applied field, that being a low energy state [36,39,40]. However, due to the finite time of the freeze-casting process and low field strength, particles tend to remain in an unaligned or partially aligned, and therefore, higher energy state [36,39]. When the alternating field is applied in conjunction with a constant field, this adds further energy to the system due to a second

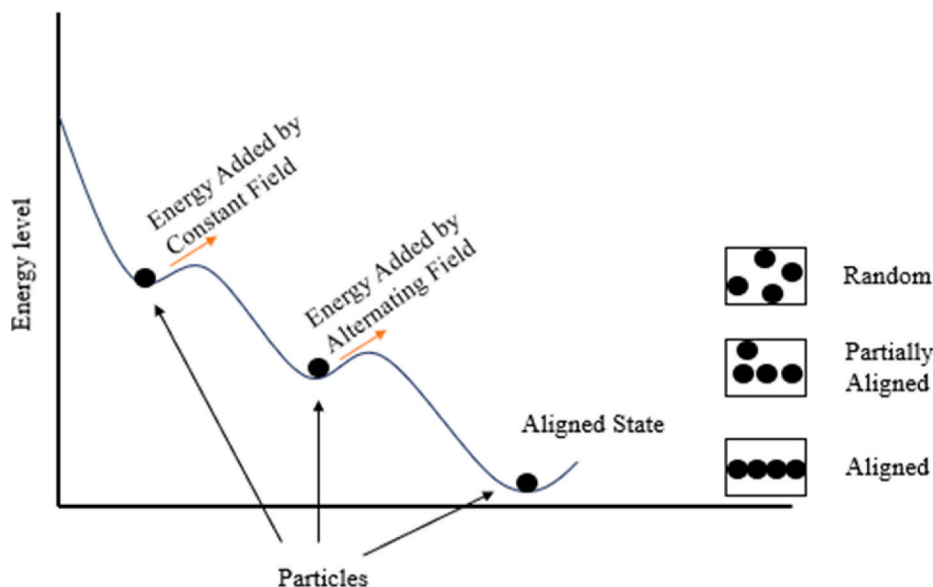


Fig. 5. Visual representation of how particles tend to remain “stuck” in higher energy states, being unable to reach the lowest energy states (i.e., alignment with the applied magnetic field) without a “push” or additional energy added to the system. The oscillating field generates this push, allowing the ferromagnetic particles to achieve an aligned or low energy state.

magnetic field, therefore more particles are able to achieve the lowest energy state where they are aligned with the magnetic field (visualized in Fig. 5). These alternating fields do also add heat in addition to a second magnetic field into the system [48,49]. However, as this is a minor increase in heat, <20 °C [48], and as large increases in heat are needed to affect the microstructure through annealing, >1000 °C [38], the magnetic field itself is primarily responsible for the alignment of the particles [40]. The alternating field provides this additional energy or “push” and allows for more organized structures, thus leading to more aligned lamellar walls, better control of the pore size and porosity, and stronger and more resilient structures.

3.2. Mechanical results

Fig. 6 displays the UCS as a function of the field type in the x- (UCS_x) and y- (UCS_y) directions. It was seen that the field type that led to the highest UCS_x was the 30% Oscillation, while No Field led to weakest UCS_x. Data of note that was reported as statistically significant was between the 30% Oscillation-No Field, with p = 4E-7, the 20% Oscillation-No Field, with p = 2.2E-5, and the 30% Oscillation-Constant

Field with p = 0.014. The p-value between Constant Field-No Field was nearly significant, at p = 0.056. From this it can be said with confidence that oscillating the field not only leads to an increase of strength from no field, but also when compared to a constant field with no alternating field, as has been done in all magnetically controlled freeze-casting research to date. The strength of the UCS_x was seen to increase with the magnitude of the oscillating field magnitude as well, which led to a strong correlation between the increase of magnitude of the oscillating field type and the strength of the material. The one notable exception was the 10% Oscillation, which did not increase in strength with an increase of the oscillating field type magnitude from the Constant Field. When looking at the UCS_y, no statistically significant differences were found as a function of the field type. From this it can be concluded that no significant change occurs to the UCS_y when different field types are applied during the freeze-casting process. No statistically significant differences were found in E_x and E_y (not pictured).

To help validate these results and build off previous research, the mechanical data above was compared to a similar, previous study [39]. It was shown in the previous study that applying a constant field led to a statistically significant higher strength in the material in the x-direction,

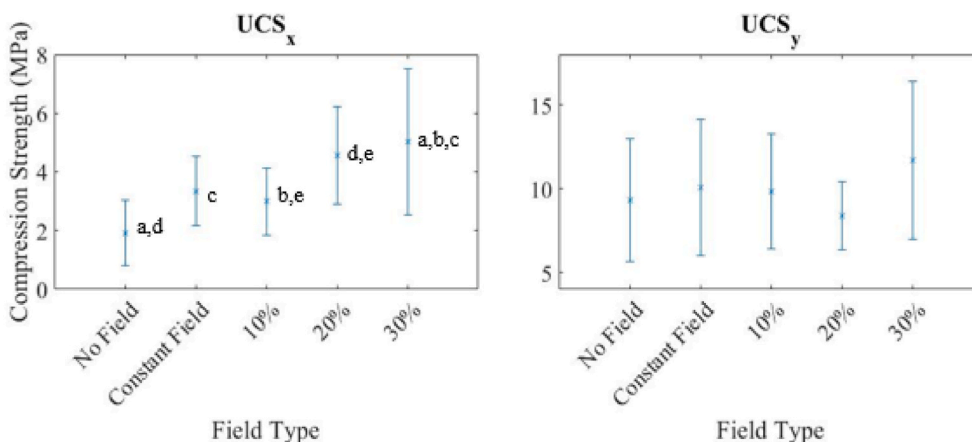


Fig. 6. Mean compression strength as a function of field type. Data presented is the mean of n = 19 measurements and the error bars represent ± one standard deviation. Pairs of means which have statistically significant differences are labeled by the same lower-case letter.

than when no field was applied. This agreed with the data in this study, as the Constant Field led to a higher compression strength than the No Field, although not quite significant at a 95% CI ($p = 0.056$). This further cemented the fact that applying magnetic fields during the freezing process of freeze casting does lead to stronger structures. Further, it was shown that applying an oscillating field led to further strengthening of the structure, even more so than applying the Constant Field. This allows for further strengthening of the structures without applying stronger magnetic fields as the alternating field allows for further alignment of the particles during freeze-casting, which translated to increased strength.

3.3. Microstructural results

Fig. 7 displays the average lamellar wall thickness as a function of the field type. The field type with the largest average wall thickness was the 30% Oscillation, while the field type with the smallest wall thickness was the 10% Oscillation. Data of note that was statistically significant was found between the wall thickness of the 30% Oscillation-Constant Field and the 20% Oscillation-Constant Field with $p = 2E-7$ and $p = 1.7E-3$, respectively. From this it was concluded that applying a constant field in conjunction with an alternating field in an orthogonal direction lead to thicker lamellar walls than simply applying a constant field, as the freezing rate remained constant between all field types, therefore any change must have been due to the only variable, the applied magnetic field. This is in line with the mechanical property results that demonstrated that applying an oscillating field led to stronger materials than simply applying a constant field. From this it would be assumed that the stronger materials would have thicker walls, thus being able to withstand more stress. This was shown to be true, as the strongest structures, the scaffolds with an oscillating field applied to them, also had the largest wall thickness.

Table 1 displays microstructural measurements of the porosity and pore area as a function of the field type. Applying the No Field led to the highest average percent porosity of each scaffold, while the 20% Oscillation led to the lowest percent porosity of each scaffold. Data of note that was statistically significant was found between the percent porosity of the No Field-10% Oscillation and No Field-20% Oscillation with $p = 0.025$ and $p = 6.3E-3$, respectively. Similarly, applying the No

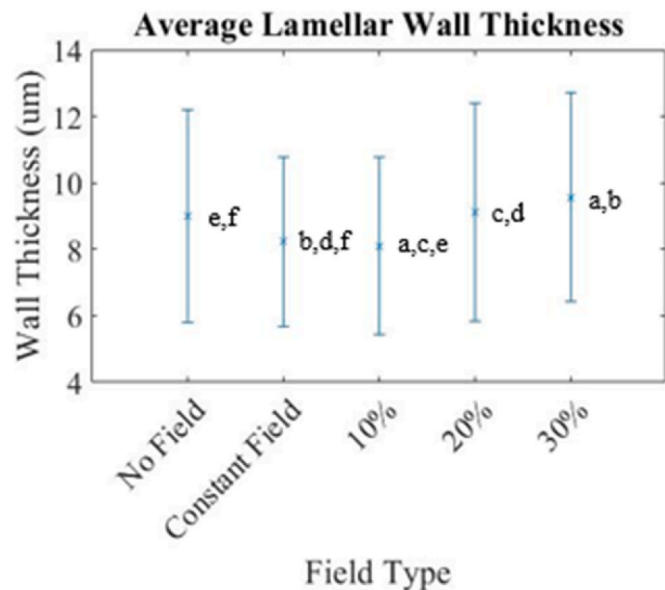


Fig. 7. Average lamellar wall thickness as a function of field type. Data presented is the mean of $n = 320$ measurements, with the error bars equal to \pm one standard deviation. Statistically significant means are noted by the same lower-case letter.

Table 1

The microstructural properties as a function of all of field types, including the area porosity, average pore area, average major axis, and average minor axis. All data is reported at $n = 5000$ measurements along with \pm one standard deviation. Statistically significant means within the same column are noted by the same lower-case letter.

Magnetic Field Type	Area Porosity (%)	Pore Area (μm^2)	Major Axis (μm)	Minor Axis (μm)
30% Oscillation	$25.1 \pm 2.9_{(a)}$	73.8 ± 10.0	$12.2 \pm 1.9_{(a)}$	4.4 ± 0.28
20% Oscillation	$20.6 \pm 3.9_{(a,b,c)}$	$59.0 \pm 16.0_{(a,b)}$	$9.6 \pm 1.9_{(a,b)}$	$4.0 \pm 0.52_{(a)}$
10% Oscillation	$21.3 \pm 2.0_{(d)}$	$61.8 \pm 7.6_{(c)}$	10.9 ± 1.4	$4.0 \pm 0.29_{(b)}$
Constant Field	$24.7 \pm 2.3_{(b)}$	$76.3 \pm 9.4_{(b)}$	$12.4 \pm 0.78_{(b)}$	4.6 ± 0.44
No Field	$25.8 \pm 2.7_{(c,d)}$	$80.3 \pm 7.5_{(a,c)}$	$11.9 \pm 1.2_{(c)}$	$4.9 \pm 0.38_{(a,b)}$

Field led to the largest average pore area, while the 20% Oscillation led to the smallest average pore area. Data of note that was statistically significant was found between the average pore area of the No Field-10% Oscillation and No Field-20% Oscillation with $p = 0.01$ and $p = 2.3E-3$, respectively. In terms of the major and minor axis, the Constant Field had the largest average major axis, while the No Field had the largest average minor axis. Data of note that was statistically significant was found between the major axis of the Constant Field-20% Oscillation with $p = 5.2E-3$, while data of note that was statistically significant was found between the minor axis of the No Field-10% Oscillation and the No Field-20% Oscillation with $p = 5.4E-4$ and $p = 4.2E-4$, respectively. The 20% Oscillation had both the smallest average major and minor axis. It was concluded that applying an oscillating field lead to lower percent porosity compared to applying no field, or only a constant field. This was most likely due to the oscillating field aligning the lamellar walls in the applied field direction thus causing less intersection and clumping between walls. This led to thicker lamellar walls, which naturally led to a lower percent porosity. Supporting this, it was shown in previous experiments that applying a magnetic field could lead to lower percent porosity [39,40] and that applying multiple fields could lead to lower average pore size [39,40].

This data also continued to validate the oscillating fields theory, as it was seen that the additional energy from the oscillating fields led to better control of the microstructures, without needing to greatly increase the magnitude of the constant field component.

3.4. Wall alignment

Fig. 8 displays SEM images and measurements of the wall alignment. With No Field, it was seen that no statistical significance was seen between any of the different directions. This was verified by looking at the SEM image in Fig. 8d as it appeared that there is no apparent order in the wall directionality. From this it can be concluded that applying no field will not lead to any change in the alignment of the lamellar walls. This agreed with previous research [39,40], and makes logical sense, as there should be no order in the alignment of the lamellar walls if no external force is applied. When applying a Constant Field or 10% Oscillation in Fig. 8b and c, respectively, it was seen that a majority of the walls are aligning at $-22.25^\circ \pm 11.25^\circ$. This was verified by inspecting the SEM images in Fig. 8e and f, respectively, as it can be seen that a majority of the lamellar walls align with that direction. When applying a 20% or 30% Oscillation, it was seen from Fig. 8g and h, respectively, that a significant majority of walls line up with $0^\circ \pm 11.25^\circ$, or the x-direction. This was verified by inspecting the SEM images in Fig. 8j and k, as it was seen that a majority of the walls line up in the x-direction.

It was shown in previous research that applying a constant field can lead to a majority of the lamellar walls aligning in the x direction [39]. Due to previously reported variability in the freeze casting process, the lamellar walls may not exactly align with the magnetic field [18]. This

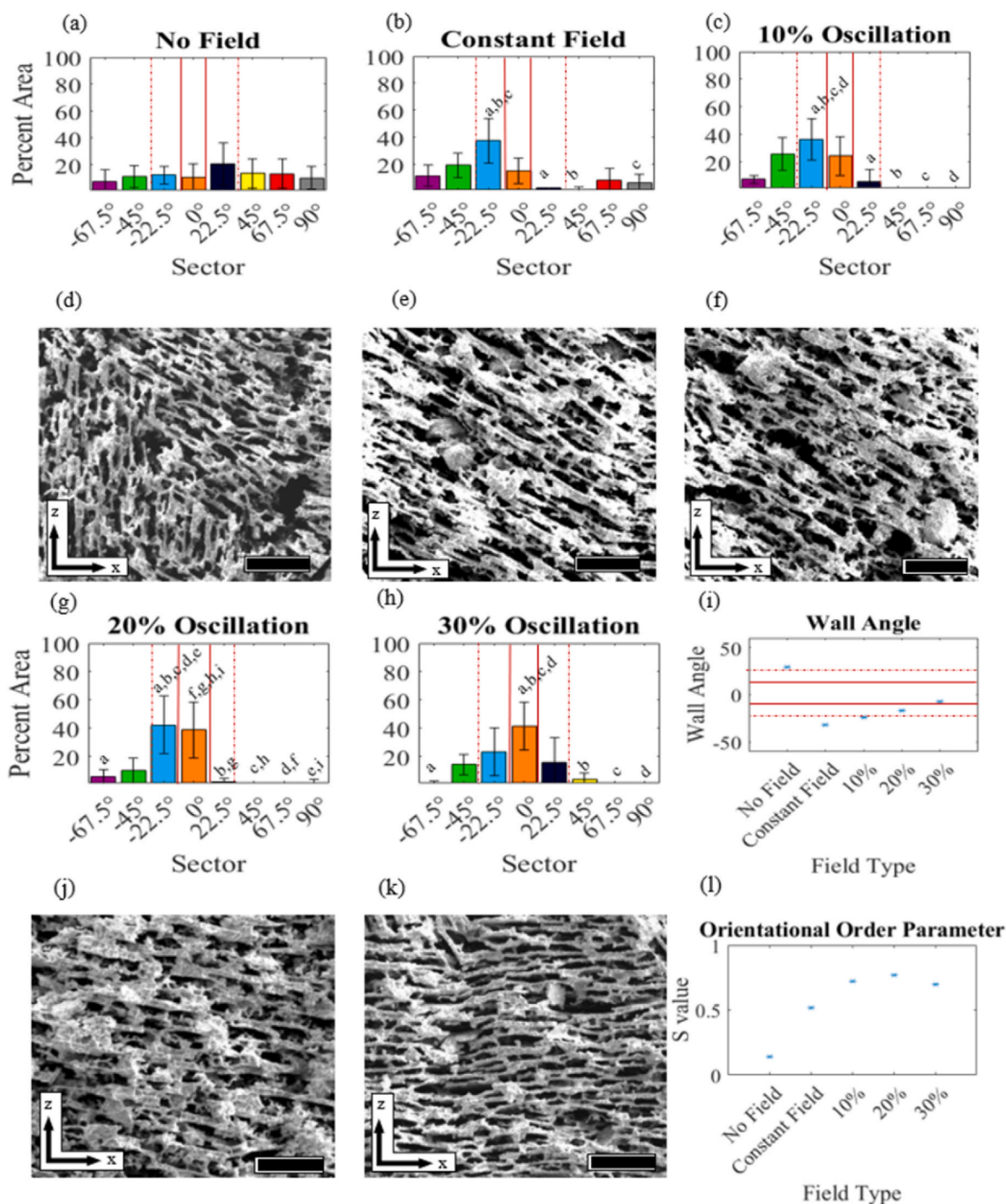


Fig. 8. Percent of walls that align within eight different sectors, those being: $-67.5^\circ \pm 11.25^\circ$, $-45^\circ \pm 11.25^\circ$, $-22.5^\circ \pm 11.25^\circ$, $0^\circ \pm 11.25^\circ$, $22.5^\circ \pm 11.25^\circ$, $45^\circ \pm 11.25^\circ$, $67.5^\circ \pm 11.25^\circ$ and $90^\circ \pm 11.25^\circ$. The x-direction corresponds with 0° and the z-direction with 90° . Plots of lamellar wall alignment and SEM images along the x-z plane for (a,d) No Field, (b,e) Constant Field, (c,f) 10% Oscillation, (g,j) 20% Oscillation, and (h,k) 30% Oscillation. (i) Plot showing the mean lamellar wall angle on the x-z plane calculated from the Q tensor. (l) Plot showing the orientational order parameter, S. All data is reported at $n = 32$ measurements along with \pm one standard deviation. Statistically significant means are noted by the same lower-case letter. The scale bars correspond to 200 μm .

was why the Constant Field and 10% Oscillation have their lamellar walls pointing near the x-direction, while the 20% and 30% Oscillation have a majority of their lamellar walls pointing directly in the x-direction.

To quantify the wall alignment throughout the samples, the approach used to quantify the (two dimensional) director order of nematic liquid crystals [50] was implemented, which is characterized by an overall alignment direction specified by a unit director vector n . Because n and $-n$ specify the same alignment direction, the amount of

ordering is described by a second-rank tensor:

$$Q = S(n \cdot n^T - \frac{I}{2}),$$

where I is the 2×2 identity. The orientational order parameter S varies from 0 when wall alignment directions are random, to 1 when all the walls are aligned in the n direction. Fig. 8i displays the angle the overall wall alignment direction n makes relative to the x-direction for different

magnetic field types. Moving from the Constant Field to the 30% Oscillation, it was seen that n gradually moves closer and closer to the x -direction with an increased alternating field magnitude. Thus, the 30% Oscillation had the closest wall alignment to the x -direction. This majority of lamellar walls lining up in the x -direction is the strengthening mechanism for the 30% Oscillation, as this field type was shown to have the strongest structures in the x -direction in Section 3.2. Fig. 8l displays the orientational order parameter S for different magnetic field types. The small value of S for No Field shows that the walls are not well-aligned with each other, while the Oscillating field types show strong alignment of lamellar wall direction with S reaching 0.77 for the 20% Oscillation and 0.70 for the 30% Oscillation. Thus this further leads to the conclusion that applying no field leads to randomness in the lamellar wall alignment. From this it was concluded that applying a magnetic field will improve the alignment of the lamellar walls, towards the x -direction, increasing microstructural control. In addition, applying an alternating field in conjunction with a constant field led to a majority of the lamellar walls aligning in the x -direction, further increasing microstructural control. In conclusion, it can be stated with confidence that applying a constant magnetic field in conjunction to an orthogonal alternating field will lead to a significant alignment and greater control of the lamellar walls.

Comparing this to previous experiments [36,39], it was also shown that applying a constant magnetic field lead to greater control of the alignment of the walls in the direction of the applied field. This study agrees with that conclusion, and further builds on the fact that the type of applied field can lead to better control of the directionality of the lamellar walls. In addition, applying the oscillating field further increased the control and alignment of the microstructure, when compared to applying the Constant Field, just as applying the Constant Field led to better control and alignment of the microstructure when compared to the No Field. This increased control and alignment of the microstructures also leads to stronger structures, as verified by the mechanical data presented here, where the strongest structures were created under the oscillating fields. This data also further validates the oscillation fields theory, as it was seen that the additional energy of the alternating field, who's magnitude is significantly lower than the constant field, increased the control over the alignment of the microstructure and lamellar walls, without needing to increase the magnitude of the constant field or change the timing or freezing rate of the freeze casting process.

These results showed that by applying an oscillating field during the freeze case process, one can increase the alignment of the microstructure and the mechanical properties of the freeze cast scaffolds without needing to increase the magnitude of the field strength. This suggests that similar techniques could be applied to other magnetic-manipulation-based fabrication techniques leading to increased alignment of the microstructure and mechanical properties of many different fabricated materials [51–53].

4. Conclusions

Based on a study of structure and properties of freeze-cast materials controlled by oscillating magnetic fields generated by a tri-axial Helmholtz coils the following conclusions can be drawn:

1. The mechanical properties of freeze-cast iron oxide scaffolds can be improved and strengthened using an alternating field in conjunction with an orthogonal constant field when compared to both no field and a constant field with no alternating field. An increase of strength up to 2x was seen when comparing the 30% Oscillation to the Constant Field, while an increase of 2.5x was seen when comparing the 30% Oscillation to the No Field.
2. The microstructure of iron oxide scaffolds can be better controlled with an oscillating magnetic field. An increase of up to 25% of the average wall thickness was seen when comparing the 30% Oscillation to the Constant Field, in addition to the average pore size of the 10% Oscillation and 20% Oscillation decreased by upwards of 25% when compared to the No Field.
3. The control of the lamellar wall alignment can increase when using an alternating field in conjunction with a constant field when compared to no field or applying only a constant field. No control of the alignment of the lamellar walls was seen when using the No Field, while the Constant Field nearly doubled the amount of alignment of walls when compared to the No Field, and the oscillating field types showing even more alignment control when compared to the Constant Field, further doubling the amount of walls aligned with the applied field.
4. Applying an oscillating field allows for an increase of the strength and microstructural control of the freeze-cast material without needing to increase the magnitude of the constant field.

Declaration of competing interest

The authors declare that they have no known competing financial interests or personal relationships that could have appeared to influence the work reported in this paper.

Acknowledgements

This work was financially supported in part by the Army Research Office under grant W911NF-21-1-0062.

References

- [1] S.W. Sofie, F. Dogan, Freeze casting of aqueous alumina slurries with glycerol, *J. Am. Ceram. Soc.* 84 (7) (2001) 1459–1464, <https://doi.org/10.1111/j.1151-2916.2001.tb00860.x>.
- [2] K. Araki, J.W. Halloran, Porous ceramic bodies with interconnected pore channels by a novel freeze casting technique, *J. Am. Ceram. Soc.* 88 (5) (2005) 1108–1114, <https://doi.org/10.1111/j.1151-2916.2005.00176.x>.
- [3] H.-D. Jung, S.-W. Yook, H.-E. Kim, Y.-H. Koh, Fabrication of titanium scaffolds with porosity and pore size gradients by sequential freeze casting, *Mater. Lett.* 63 (17) (2009) 1545–1547, <https://doi.org/10.1016/j.matlet.2009.04.012>.
- [4] H.-D. Jung, S.-W. Yook, T.-S. Jang, Y. Li, H.-E. Kim, Y.-H. Koh, Dynamic freeze casting for the production of porous titanium (Ti) scaffolds, *Mater. Sci. Eng. C* 33 (1) (2013) 59–63, <https://doi.org/10.1016/j.msec.2012.08.004>.
- [5] Y. Chino, D.C. Dunand, Directionally freeze-cast titanium foam with aligned, elongated pores, *Acta Mater.* 56 (1) (2008) 105–113, <https://doi.org/10.1016/j.actamat.2007.09.002>.
- [6] J.C. Li, D.C. Dunand, Mechanical properties of directionally freeze-cast titanium foams, *Acta Mater.* 59 (1) (2011) 146–158, <https://doi.org/10.1016/j.actamat.2010.09.019>.
- [7] H.-W. Kang, Y. Tabata, Y. Ikada, Fabrication of porous gelatin scaffolds for tissue engineering, *Biomaterials* 20 (14) (1999) 1339–1344, [https://doi.org/10.1016/S0142-9612\(99\)00036-8](https://doi.org/10.1016/S0142-9612(99)00036-8).
- [8] H. Schoof, J. Apel, I. Heschel, G. Rau, Control of pore structure and size in freeze-dried collagen sponges, *J. Biomed. Mater. Res.* 58 (4) (2001) 352–357, <https://doi.org/10.1002/jbm.1028>.
- [9] M.V. Dinu, M. Prádný, E.S. Drágan, J. Michálek, Ice-templated hydrogels based on chitosan with tailored porous morphology, *Carbohydr. Polym.* 94 (1) (2013) 170–178, <https://doi.org/10.1016/j.carbpol.2013.01.084>.
- [10] N.L. Francis, et al., An ice-templated, linearly aligned chitosan-alginate scaffold for neural tissue engineering, *J. Biomed. Mater. Res.* 101 (12) (2013) 3493–3503, <https://doi.org/10.1002/jbm.a.34668>.
- [11] T. Köhnke, T. Elder, H. Theliander, A.J. Ragauskas, Ice templated and cross-linked xylan/nanocrystalline cellulose hydrogels, *Carbohydr. Polym.* 100 (2014) 24–30, <https://doi.org/10.1016/j.carbpol.2013.03.060>.
- [12] S. Deville, E. Saiz, A.P. Tomsia, Ice-templated porous alumina structures, *Acta Mater.* 55 (6) (2007) 1965–1974, <https://doi.org/10.1016/j.actamat.2006.11.003>.
- [13] S. Deville, E. Saiz, A.P. Tomsia, Freeze casting of hydroxyapatite scaffolds for bone tissue engineering, *Biomaterials* 27 (32) (2006) 5480–5489, <https://doi.org/10.1016/j.biomaterials.2006.06.028>.
- [14] E. Munch, J. Franco, S. Deville, P. Hunger, E. Saiz, A.P. Tomsia, Porous ceramic scaffolds with complex architectures, *JOM (J. Occup. Med.)* 60 (6) (2008) 54–58, <https://doi.org/10.1007/s11837-008-0072-5>.
- [15] T.A. Ogden, Bioinspired Ultrasound Freeze Casting: Engineered Porous Scaffolds through Freeze Casting and Ultrasound Directed Self-Assembly, M.S., The University of Utah, United States – Utah, 2019. Aug. 25, 2021. [Online]. Available: <https://www.proquest.com/docview/2496206030/abstract/4F4366FD0D0E4001PQ/1>.

- [16] S.E. Naleway, et al., Bioinspired composites from freeze casting with clathrate hydrates, *Mater. Des.* 71 (2015) 62–67, <https://doi.org/10.1016/j.matdes.2015.01.010>. Apr.
- [17] S. Roy, A. Wanner, Metal/ceramic composites from freeze-cast ceramic preforms: domain structure and elastic properties, *Compos. Sci. Technol.* 68 (5) (2008) 1136–1143, <https://doi.org/10.1016/j.compscitech.2007.06.013>. Apr.
- [18] S.E. Naleway, K.C. Fickas, Y.N. Maker, M.A. Meyers, J. McKittrick, Reproducibility of ZrO₂-based freeze casting for biomaterials, *Mater. Sci. Eng. C* 61 (2016) 105–112, <https://doi.org/10.1016/j.msec.2015.12.012>. Apr.
- [19] S. Sofie, Fabrication of functionally graded and aligned porosity in thin ceramic substrates with the novel freeze–tape-casting process, *J. Am. Ceram. Soc.* 90 (7) (2007) 2024–2031, <https://doi.org/10.1111/j.1551-2916.2007.01720.x>.
- [20] L. Qian, H. Zhang, Controlled freezing and freeze drying: a versatile route for porous and micro-/nano-structured materials, *J. Chem. Technol. Biotechnol.* 86 (2) (2011) 172–184, <https://doi.org/10.1002/jctb.2495>.
- [21] M.B. Frank, et al., Synergistic structures from magnetic freeze casting with surface magnetized alumina particles and platelets, *J. Mech. Behav. Biomed. Mater.* 76 (2017) 153–163, <https://doi.org/10.1016/j.jmbbm.2017.06.002>. Dec.
- [22] P. M. Hunger, A. E. Donius, and U. G. K. Wegst, “Platelets self-assemble into porous nacre during freeze casting,” *J. Mech. Behav. Biomed. Mater.*, vol. 19, pp. 87–93, Mar. 2013, doi: 10.1016/j.jmbbm.2012.10.013.
- [23] S. Deville, et al., In situ X-ray radiography and tomography observations of the solidification of aqueous alumina particle suspensions—Part I: initial instants, *J. Am. Ceram. Soc.* 92 (11) (2009) 2489–2496, <https://doi.org/10.1111/j.1551-2916.2009.03163.x>.
- [24] S. Deville, et al., Metastable and unstable cellular solidification of colloidal suspensions, *Nat. Mater.* 8 (12) (2009) 966–972, <https://doi.org/10.1038/nmat2571>. Dec.
- [25] P.M. Hunger, A.E. Donius, U.G.K. Wegst, Structure–property-processing correlations in freeze-cast composite scaffolds, *Acta Biomater.* 9 (5) (2013) 6338–6348, <https://doi.org/10.1016/j.actbio.2013.01.012>. May.
- [26] A. Preiss, B. Su, S. Collins, D. Simpson, Tailored graded pore structure in zirconia toughened alumina ceramics using double-side cooling freeze casting, *J. Eur. Ceram. Soc.* 32 (8) (2012) 1575–1583, <https://doi.org/10.1016/j.jeurceramsoc.2011.12.031>. Jul.
- [27] H. Bai, Y. Chen, B. Delattre, A.P. Tomsia, R.O. Ritchie, Bioinspired large-scale aligned porous materials assembled with dual temperature gradients, *Sci. Adv.* 1 (11) (2015) e1500849, <https://doi.org/10.1126/sciadv.1500849>. Dec.
- [28] H. Bai, et al., Bioinspired hydroxyapatite/poly(methyl methacrylate) composite with a nacre-mimetic architecture by a bidirectional freezing method, *Adv. Mater.* 28 (1) (2016) 50–56, <https://doi.org/10.1002/adma.201504313>.
- [29] H. Bai, et al., Biomimetic gradient scaffold from ice-templating for self-seeding of cells with capillary effect, *Acta Biomater.* 20 (2015) 113–119, <https://doi.org/10.1016/j.actbio.2015.04.007>. Jul.
- [30] J.-W. Moon, H.-J. Hwang, M. Awano, K. Maeda, Preparation of NiO–YSZ tubular support with radially aligned pore channels, *Mater. Lett.* 57 (8) (2003) 1428–1434, [https://doi.org/10.1016/S0167-577X\(02\)01002-9](https://doi.org/10.1016/S0167-577X(02)01002-9). Feb.
- [31] Y. Tang, Q. Miao, S. Qiu, K. Zhao, L. Hu, Novel freeze-casting fabrication of aligned lamellar porous alumina with a centrosymmetric structure, *J. Eur. Ceram. Soc.* 34 (15) (2014) 4077–4082, <https://doi.org/10.1016/j.jeurceramsoc.2014.05.040>. Dec.
- [32] Y. Tang, S. Qiu, Q. Miao, C. Wu, Fabrication of lamellar porous alumina with axisymmetric structure by directional solidification with applied electric and magnetic fields, *J. Eur. Ceram. Soc.* 36 (5) (2016) 1233–1240, <https://doi.org/10.1016/j.jeurceramsoc.2015.12.012>. Apr.
- [33] M.M. Porter, et al., Torsional properties of helix-reinforced composites fabricated by magnetic freeze casting, *Compos. Struct.* 119 (2015) 174–184, <https://doi.org/10.1016/j.compstruct.2014.08.033>. Jan.
- [34] M.B. Frank, et al., Stiff, porous scaffolds from magnetized alumina particles aligned by magnetic freeze casting, *Mater. Sci. Eng. C* 77 (2017) 484–492, <https://doi.org/10.1016/j.msec.2017.03.246>. Aug.
- [35] M.M. Porter, et al., Magnetic freeze casting inspired by nature, *Mater. Sci. Eng. A* 556 (2012) 741–750, <https://doi.org/10.1016/j.msea.2012.07.058>. Oct.
- [36] I. Nelson, et al., Freeze-casting of surface-magnetized iron(II,III) oxide particles in a uniform static magnetic field generated by a Helmholtz coil, *Adv. Eng. Mater.* 21 (3) (2019) 1801092, <https://doi.org/10.1002/adem.201801092>.
- [37] M.M. Porter, P. Niksiar, J. McKittrick, Microstructural control of colloidal-based ceramics by directional solidification under weak magnetic fields, *J. Am. Ceram. Soc.* 99 (6) (2016) 1917–1926, <https://doi.org/10.1111/jace.14183>.
- [38] I. Nelson, S.E. Naleway, Intrinsic and extrinsic control of freeze casting, *J. Mater. Res. Technol.* 8 (2) (2019) 2372–2385, <https://doi.org/10.1016/j.jmrt.2018.11.011>. Apr.
- [39] I. Nelson, L. Gardner, K. Carlson, S.E. Naleway, Freeze casting of iron oxide subject to a tri-axial nested Helmholtz-coils driven uniform magnetic field for tailored porous scaffolds, *Acta Mater.* 173 (2019) 106–116, <https://doi.org/10.1016/j.actamat.2019.05.003>. Jul.
- [40] I. Nelson, et al., Helical and bouligand porous scaffolds fabricated by dynamic low strength magnetic field freeze casting, *JOM (J. Occup. Med.)* 72 (4) (2020) 1498–1508, <https://doi.org/10.1007/s11837-019-04002-9>. Apr.
- [41] J.J. Abbott, Parametric design of tri-axial nested Helmholtz coils, *Rev. Sci. Instrum.* 86 (5) (2015), <https://doi.org/10.1063/1.4919400>, 054701, May.
- [42] B. Liu, L. Xu, Y. Liu, J. Wang, J. Wang, Q. Fang, Effect of cold working and annealing on microstructure and properties of powder metallurgy high entropy alloy, *Sci. China Technol. Sci.* 61 (2) (2018) 197–203, <https://doi.org/10.1007/s11431-017-9122-5>. Feb.
- [43] B. Morales-Castañeda, D. Zaldívar, E. Cuevas, O. Maciel-Castillo, I. Aranguren, F. Fausto, An improved Simulated Annealing algorithm based on ancient metallurgy techniques, *Appl. Soft Comput.* 84 (2019) 105761, <https://doi.org/10.1016/j.asoc.2019.105761>. Nov.
- [44] L.N. Ramanathan, J.W. Jang, J.K. Lin, D.R. Frear, Solid-state annealing behavior of two high-Pb solders, 95Pb5Sn and 90Pb10Sn, on Cu under bump metallurgy, *J. Electron. Mater.* 34 (10) (2005) L43–L46, <https://doi.org/10.1007/s11664-005-0262-7>. Oct.
- [45] L. Li, et al., Microstructure and mechanical property evolution during annealing of a cold-rolled metastable powder metallurgy high entropy alloy, *Entropy* 21 (9) (2019) 833, <https://doi.org/10.3390/e21090833>. Aug.
- [46] G.F. Carter, D.E. Paul, G.F. Carter, *Materials Science And Engineering. Materials Park, UNITED STATES: A S M International*, 1991. Sep. 18, 2021. [Online]. Available: <http://ebookcentral.proquest.com/lib/utah/detail.action?docID=3002464>.
- [47] A. Rollett, G.S. Humphreys, M. Hatherly, Recrystallization and Related Annealing Phenomena, 2004. <https://web.a.ebscohost.com/ehost/ebookviewer/ebook?sid=e1076163-3299-40af-b896-59f41fc5564b%40sessionmgr4006&vid=0&format=EB>. (Accessed 22 September 2021).
- [48] K. Kan-Dapaah, N. Rahbar, W. Soboyejo, Novel magnetic heating probe for multimodal cancer treatment, *Med. Phys.* 42 (5) (2015) 2203–2211, <https://doi.org/10.1118/1.4915955>.
- [49] K. Kan-Dapaah, N. Rahbar, W. Soboyejo, Implantable magnetic nanocomposites for the localized treatment of breast cancer, *J. Appl. Phys.* 116 (23) (2014) 233505, <https://doi.org/10.1063/1.4903736>. Dec.
- [50] J.V. Selinger, *Introduction to the Theory of Soft Matter: from Ideal Gases to Liquid Crystals*, Springer, Cham, 2016.
- [51] F. Khademolhosseini, M. Chiao, Fabrication and patterning of magnetic polymer micropillar structures using a dry-nanoparticle embedding technique, *J. Microelectromechanical Syst.* 22 (1) (2013) 131–139, <https://doi.org/10.1109/JMEMS.2012.2218576>. Feb.
- [52] H. Akiyama, A. Ito, Y. Kawabe, M. Kamihira, Fabrication of complex three-dimensional tissue architectures using a magnetic force-based cell patterning technique, *Biomed. Microdevices* 11 (4) (2009) 713–721, <https://doi.org/10.1007/s10544-009-9284-x>. Aug.
- [53] F. Fan, et al., Rotating magnetic field-controlled fabrication of magnetic hydrogel with spatially disk-like microstructures, *Sci. China Mater.* 61 (8) (2018) 1112–1122, <https://doi.org/10.1007/s40843-017-9221-4>. Aug.